Tritium Accountancy and Safety Case for Molten Salt Liquid Immersion Blanket

National Laboratory Principal Investigator	Idaho National Laboratory Adriaan Riet adriaan.riet@inl.gov
Company Principal Investigator	Commonwealth Fusion Systems Brandon Sorbom brandon@cfs.energy
Award	INFUSE 2020
Period of Performance	01/14/2021 – 03/31/2023
Final Report Submission Date	

1 Technical Overview

1.1 Problem Statement

Describe the CFS challenges this program is meant to address. Should be adapted from original application, noting any departures / evolutions from that original application.

CFS and INL developed this project to characterize the expected distribution and migration of tritium throughout the ARC power plant, including in the torus and primary FLiBe salt loop. While other work has investigated the tritium inventory associated with the tritium processing plant envisioned for ARC, there has not yet been a rigorous estimate of the tritium inventory associated with the solid materials in the torus and the primary salt loop. This work will not consider the tritium inventory associated with the tritium processing plant, and when the "inventory" is discussed here it does not include that. Understanding the tritium distribution in the published 2018 ARC paper [1] is a key first step to minimizing the inventory in the eventual final ARC plant. This report will refer to ARC-2018 to denote the fact that the Kuang 2018 design paper is used for ARC modeling.

Furthermore, the project was motivated by a desire to understand tritium permeation through the salt loop into outer tritium containment system, both during nominal steady-state operations and during important accident scenarios. The project proposal laid out the following steps:

- Leverage INL's MELCOR/TMAP code to characterize tritium transport and safety behavior for an ARC-2018 design using FLiBe
- Characterize steady-state analysis of tritium transport in ARC-2018 and its ancillary systems
- Conduct Loss-of-Flow Accident (LOFA) analysis scenarios in which forced convection is lost but there are no coolant leaks. This step was eventually excluded from the project for technical reasons.
- Perform Lost-of-Coolant-Accident (LOCA) analysis during accident progression to assess feasibility of radiation or alternate strategies for decay heat removal in event of LOCA in ARC-2018. This step was eventually excluded from the project for technical reasons.

The first two steps were carried out at INL and the results are shown below. Due to the need for further developments in the MELCOR/TMAP code and a need for additional information to account for decay heat, the third and fourth steps were attempted but further work is needed in a subsequent project to achieve satisfactory results.

1.2 Work Scope

Describe the approach used to achieve the project goals, including the capabilities at the national laboratory or partner facility, as well as the capabilities at CFS and its subcontractors on this award. Can be informed / adapted from original application, noting departures / evolutions.

ARC is in the preliminary design stages and one of the major design objectives for the facility is to minimize the required tritium inventory. A major purpose of this study is to conduct preliminary modeling to determine which components and input parameters have the largest impact on required tritium inventory so that further study and development can focus on those components and input parameters that have the largest impact on minimizing the total tritium inventory. To accomplish this, the INL team used the geometry and heat loads laid out in the ARC 2018 paper.

MELCOR-TMAP, a system-level engineering and safety analysis code developed at INL, was used for this project due to its capability of modeling time-dependent conjugate heat transfer and tritium transport. The code integrates the thermal-hydraulic and radionuclide capabilities of the well-established MELCOR reactor safety code with the hydrogen species transport capabilities of TMAP4. MELCOR/TMAP is thus capable of accurately modeling the unique physics and operating conditions of fusion device environments, making it an ideal candidate for modeling the ARC device. The MELCOR/TMAP code has the limitation of utilizing a one-dimensional nodalization scheme; however, three-dimensional geometries can be emulated based on the arrangement of volumes, flow paths, and walls. This has the advantage of producing computationally efficient solutions for large systems but with the disadvantage of a coarser spatial fidelity as compared to computational fluid dynamics (CFD) or other two- and three-dimensional codes. Another limitation is that the correlations used in the systems-level code are experimentally determined, and only valid in their regions of applicability.

Toward achieving the accepted technical goals for this project, INL created an input file for use in MELCOR/TMAP based on preliminary design specifications of the ARC device provided by CFS. The computational model specified in this input file includes the most vital components within the vacuum vessel in the ARC-2018 device design, including breeding blankets, coolant channels, shielding and containment walls, and plasma chamber. In addition, a simplified heat exchanger and tritium extractor system were modeled. Instead of modeling the magnetohydrodynamics of the plasma within MELCOR/TMAP, tritium source terms were implemented in the plasma-facing walls based on neutronics modeling and simulations performed by CFS.

Volumes of fluid (liquid, gas, or a mixture) are represented in MELCOR/TMAP using MELCOR's Control Volume Hydrodynamics (CVH) package, and connections where mass transfer occurs between control volumes are made using the Flow Path (FL) package. These packages include the physics necessary to model the thermodynamics and hydrodynamics between control volumes as well as mass transfer correlations that are used in other packages in MELCOR/TMAP. Hydrogen species transport is handled using the TMAP capabilities which have been integrated with the MELCOR Heat Slab (HS) package to calculate species transport through solid walls. The HS package is capable of modeling heat transfer and hydrogen transport through composite material walls including those with very thin films (less than 1 micron). Material properties which are necessary for the various MELCOR/TMAP packages and physics were included in the input file. These properties for the FLiBe breeder / coolant as well as tungsten, Inconel-718 nickel alloy, steel, and other solid structure materials were taken from reliable data available in the literature. The most important properties included in the input file are the geometries which represent the

physical dimensions of the device, thermophysical properties (density, thermal conductivity, specific heat) and parameters for hydrogen transport (solubility, diffusivity, recombination, trap energies and densities). The quantities for which there exist the highest levels of uncertainty are the tritium transport properties such as solubility and diffusivity; the following section describes how a range of these values are chosen to determine the sensitivity of the MELCOR-TMAP model to these input parameters.

As uncertainties for tritium transport properties can range up to several orders of magnitude for a single parameter, it was necessary to determine the effect of these uncertainties on tritium transport calculations. Simulations were run for determining the inventory and permeation rate of tritium from the salt loop using differing sets of hydrogen transport parameters for FLiBe and tungsten. Transport properties for FLiBe were taken from Calderoni et al. [2], Nakamura et al. [3], and Malinauskas and Richardson [4]. Solubility and diffusivity parameters for tungsten were taken from Frauenfelder [5], Heinola & Ahlgren [6], and Esteban et al. [7], while recombination parameters for tungsten were taken from Anderl et al [8]. The solubility values for Heinola & Ahlgren were derived by dividing the permeability values from Frauenfelder and dividing them by the diffusivity values of Heinola & Ahlgren. However, since these calculated solubility values closely resemble those from Frauenfelder over the same temperature range, they are included for comparison in the following figures but were not used for simulations.

In these figures the transport properties are plotted in the original temperature ranges provided from the literature. However, these follow an Arrhenius equation of the form $y = A * exp\,[-\frac{B}{T}]$ where y is the transport property, A and B are constants, and T is temperature in Kelvin. These properties are input into MELCOR/TMAP in this same form to allow for interpolation or extrapolation to the temperature of the materials in the simulations. For the simulations performed of the ARC-2018 device, tungsten on the plasma-facing walls ranged in temperature from 800 to 1650 K.

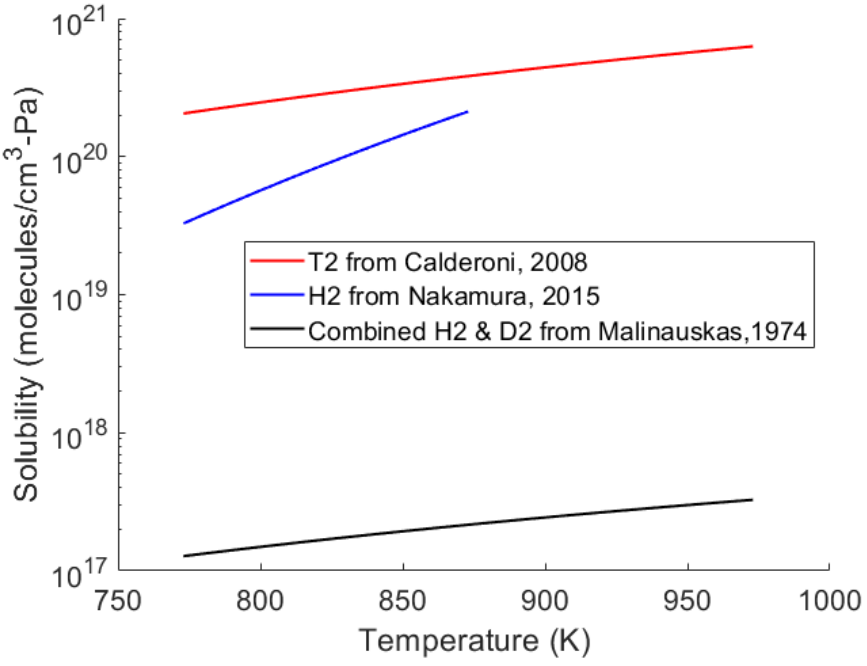

Figure 1.2.1. Solubility values used for FLiBe.

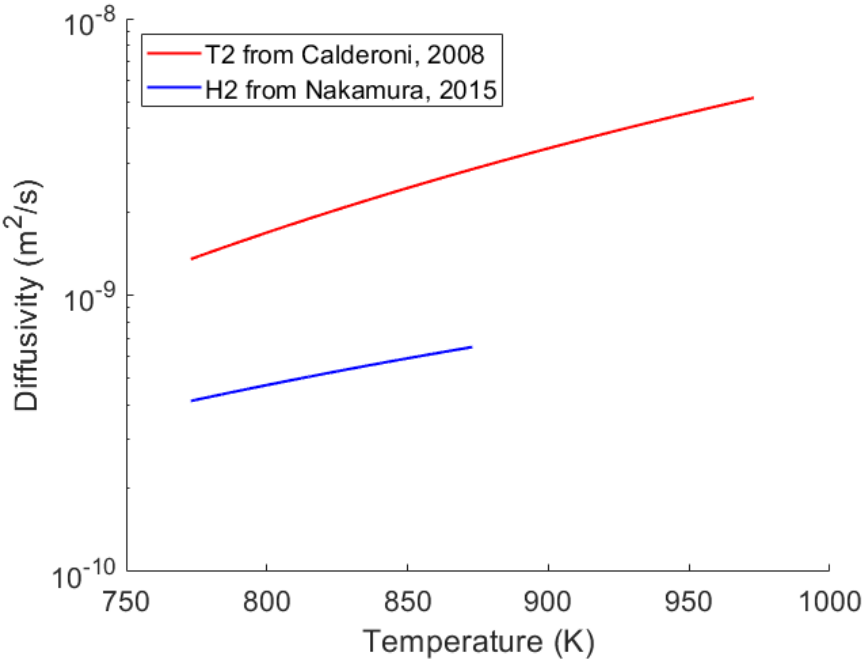

Figure 1.2.2. Diffusivity values used for FLiBe.

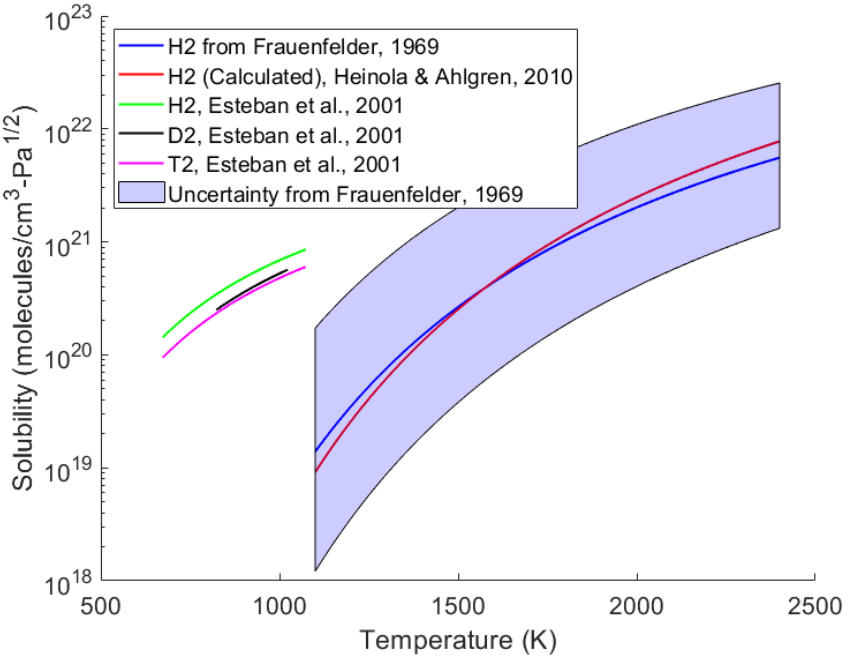

Figure 1.2.3. Solubility values used for tungsten.

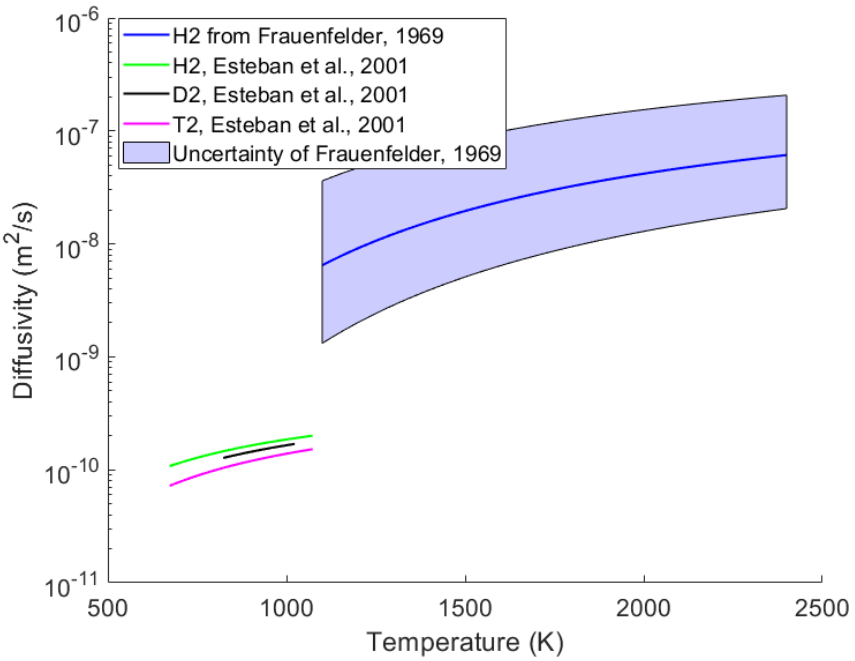

Figure 1.2.4. Diffusivity values used for tungsten.

Included below in Table 1.2.1 are the tasks and timeline associated with INL's role in this project. The results of these tasks are discussed to follow.

Table 1.2.1. Tasks and deliverables.

Task No.	Tasks	INL Role/Responsibilities	Timeline (Months)
1	Neutronics Calculations	INL will provide participant any necessary guidance on neutronic outputs needed for MELCOR analysis.	1-2
2	Steady-State Tritium Transport Analysis	INL will perform steady-state tritium transport analysis for ARC-2018 with MELCOR/TMAP or equivalent.	1-15
3	~~LOFA Analysis~~	INL will simulate a loss-of-flow accident in ARC-2018 with MELCOR, based on neutronic, activation, and design details provided by CFS. This activity was not completed.	6-20
4	~~LOCA Analysis~~	INL will simulate a loss-of-coolant accident in ARC-2018 with MELCOR, based on neutronic, activation, and design details provided by CFS. This activity was not completed.	9-20

Task 1 was completed at the early stages of the project in collaboration with CFS. The input file based on the ARC-2018 device for use with MELCOR/TMAP was created for use in steady state calculations in the following task. The tritium flux values used in the MELCOR/TMAP input file were provided from CFS based on neutronics simulations.

Task 2 was completed following the creation of the MELCOR/TMAP input file based on the ARC-2018 device design specifications and performing simulations for various test cases.

As part of Task 2, a characterization study of the tritium permeation through the heat exchanger as a function of extraction efficiency was performed. Efficiencies for the tritium extraction system were varied between 10% up to 99.99%, and the resulting tritium permeation across the heat exchanger to the environment were calculated.

For another set of simulations, a small tungsten layer of varying thickness was added to the heat exchanger pipe touching the FLiBe. This was done to determine the effectiveness of reduction in tritium permeation through the heat exchanger walls with the addition of the tungsten layer. The thickness for the tungsten layer varied between 1 micron and 100 microns.

The original project plans included analysis work of a Loss of Flow accident (Task 3). However, due to timing constraints, this analysis has been reserved for future work. A future analysis could consider the following aspects:

- Decay heat expected for the various activated components within the tokamak
- Degree of natural convection that might promote heat exhaust even without active cooling systems, depending on the type of accident scenario considered
- Tritium release rates as functions of both temperature due to decay heat but also tritium trap site models for irradiated tungsten and in-vessel components

Task 4 was not completed due to the discovery of further developments that were needed in MELCOR-TMAP to achieve reliable results.

The following section will discuss the results of tasks 1 and 2.

References:

[1] Kuang, A. Q., Cao, N. M., Creely, A. J., Dennett, C. A., Hecla, J., LaBombard, B., Tinguely, R. A., Tolman, E. A., Hoffman, H., Major, M., Ruiz Ruiz, J., Brunner, D., Grover, P., Laughman, C., Sorbom, B. N., & Whyte, D. G. (2018). Conceptual design study for heat exhaust management in the ARC fusion pilot plant. *Fusion Engineering and Design*, *137*, 221–242. https://doi.org/10.1016/j.fusengdes.2018.09.007

[2] P. Calderoni, P. Sharpe, M. Hara, and Y. Oya, "Measurement of tritium permeation in flibe (2LiF-BeF2)," *Fusion Eng. Des.*, vol. 83, no. 7-9, pp. 1331-1334, Dec. 2008, doi: 10.1016/j.fusengdes.2008.05.016.

[3] A. Nakamura, S. Fukada, and R. Nishiumi, "Hydrogen isotopes permeation in a fluoride molten salt for nuclear fusion blanket," *J. Plasma Fusion Res. Series*, vol. 11, no. 25, 2015.

[4] A.P. Malinauskas, D.M. Richardson, "The solubilities of hydrogen, deuterium, and helium in molten Li2BeF4," *Ind. Eng. Chem. Fundam.*, vol. 13, no. 3, Aug. 1974.

[5] R. Frauenfelder, "Solution and diffusion of hydrogen in tungsten," *J. Vac. Sci. Technol.*, vol. 6, no. 3, pp. 388-397, May 1969, doi: 10.1116/1.1492699.

[6] K. Heinola and T. Ahlgren, "Diffusion of hydrogen in bcc tungsten studied with first principle calculations," *J. Appl. Phys.*, vol. 107, no. 11, pp. 113531-1-113531-8, Jun. 2010, doi: 10.1063/1.3386515.

[7] G.A. Esteban, A. Perujo, L.A. Sedano, and K. Douglas, "Hydrogen isotope diffusive transport parameters in pure polycrystalline tungsten," *J. Nucl. Mater.*, vol. 295, no. 1, pp. 49-56, May 2001, doi: 10.1016/S0022-3115(01)00486-X.
[8] R.A. Anderl, D.F. Holland, G.R. Longhurst, R.J. Pawelko, C.L. Trybus, and C.H. Sellers, "Deuterium transport and trapping in polycrystalline tungsten," *Fusion Technol.*, vol. 21, no. 2P2, Mar. 1992, doi: 10.13182/FST92-A29837.

1.3 Results

Describe the tasks accomplished, results obtained, key deliverables, lessons learned.

1.3.1 Model Description

For the results reported in this section, a base test case was run with fixed tritium transport properties, flow conditions, and tritium extraction system efficiency against which the remaining test cases were compared. For each of the following results sections, this base test case is listed as "Base" and the remaining test cases are modified from this test case with the relevant modified parameter(s). The parameters for the material properties for the base case are included in Table 1.3.2.

Table 1.3.2. Parameters for "Base" case and associated figure as applicable.

Material	**Solubility**	**Diffusivity**	**Recombination**	**Thermophysical Properties**
FLiBe	Nakamura et al. [1], Fig. 1.2.1	Calderoni et al. [2], Fig. 1.2.2	N/A	Humrickhouse & Merrill [3]
Tungsten	Frauenfelder [4], Fig. 1.2.3	Frauenfelder [4], Fig. 1.2.4	Anderl et al. [5]	
Inconel-718	Robertson [6]	Robertson [6]	Non-oxidized Incoloy 800, Esteban et al. [7]	Agazhanov et al. [8]
Berylliu m	Shapovalov & Dukel'skii [9]	Shapovalov & Dukel'skii [9]	Abramov et al. [10]	ITER [11]

Apart from the material property settings, several other assumptions were made in the creation of the input file based on the ARC-2018 design. The most notable assumptions made include the following:

1. The transfer of tritium from the pool (liquid) to atmosphere (gaseous) phase within a single control volume (CV) was considered negligible as compared to the transfer through vessel walls; thus, liquid-to-atmosphere transfer of hydrogen species within the same CV was disabled. Physically, this is a reasonable assumption since most internal volumes where FLiBe exists (such as in the coolant channels and blanket) in the ARC-2018 device are

filled with liquid FLiBe only. However, since the CVH module in the MELCOR/TMAP code requires that a small portion of each CV contain an atmosphere phase volume, a very small portion of the liquid volume in each CV (approximately 1 percent or less) was replaced with gas. This replacement is assumed to have a negligible effect on tritium transport to and from the CV, and since pool to atmosphere transfer of tritium is disabled, no tritium is transported from the liquid to atmosphere phase within each CV.

2. At the time of code compilation, MELCOR/TMAP can be run in two different modes: One mode has additional physics built in to deal with the very particular behavior of aerosols (including thermophoresis and bend deposition) and material oxidation/corrosion, and one mode omits these physical effects for simplicity and computational speed. Since neither set of physics (aerosol nor material oxidation) is expected to be relevant to the questions of interest in this project, the simpler mode was used. Several steady-state simulations were run in the more detailed mode to validate that these additional physical effects were not relevant and had no effect.
3. Gas trapping was enabled in all HSs for tritium only; trapping for protium, deuterium, and helium species was disabled. This is a reasonable assumption because only tritium transport is considered in these simulations; mixed molecular species (HT, DT, HD) are not considered. The trap parameters used in the simulations for tungsten and beryllium follow those provided by Hodille et al. [12] and Billone et al. [13], respectively, and are provided in Table 1.3.3. It is assumed that the difference in tungsten trap energies at the FW layers differ primarily in the 1.50 eV ion-induced trap sites which increase in density as a function of tritium fluence [12]. The tungsten lining in the heat exchanger (HX) in the results in this report are the same as those used in the FW lining which do not include the 1.50 eV trap sites; however, in reality, the 1.65, 1.85, and 2.06 eV trap sites which exist as a result of neutron damage at the FW should also be excluded from the HX tungsten lining. However, examining simulations with varying tritium extraction efficiency of the HX tungsten lining which include these trap sites as compared to those without these trap sites, the additional trap sites result in less than a 4 mg or 3.0% increase in trapped inventory in the HX. This additional trapped inventory due to these trap sites induced by neutron damage results in less than a 0.01% increase in the total ARC-2018 device trapped inventory. Thus, the change in inventory due to these additional trap sites in the HX tungsten layer is considered to be insignificant as compared to the local and total inventory, though it may be a subject for future study.
4. As MELCOR/TMAP is not designed with magnetohydrodynamics (MHD) or other modeling capabilities for plasma, implantation particle sources are used as tritium sources. These are used in HSs for the first wall of the inner vacuum vessel and in the beryllium and Inconel-718 layers in the outer vacuum vessel. Tritium sources also exist in the control volumes in FLiBe coolant channels and blankets throughout the device. These source values have been provided by CFS based on results of neutronics simulations of the ARC-2018 device [14], with a total tritium source rate of 9.88×10^{-7} kg/s.
5. The tritium extraction system has been simplified to extract a certain percentage of tritium from the hot leg stream exiting the device. The baseline efficiency for this system is set to 90%.

Table 1.3.3. Trapping energies and densities for tungsten and beryllium used in the MELCOR/TMAP model.

Material	Trap Energy (eV)	Trap Density	Reference

		(atomic percent)	
Tungsten at First Wall	0.85	0.13	Hodille et al. [12]
	1.00	0.035	
	1.50	8.00	
	1.65	0.1	
	1.85	0.2	
	2.06	0.05	
Tungsten near First Wall	0.85	0.13	
	1.00	0.035	
	1.50	1.00	
	1.65	0.1	
	1.85	0.2	
	2.06	0.05	
Tungsten far from First Wall (including tungsten in HX coating)	0.85	0.13	
	1.00	0.035	
	1.65	0.1	
	1.85	0.2	
	2.06	0.05	
Beryllium	1.00	0.1	Billone et al. [13]

	1.80	0.1	

The geometry of ARC-2018 is divided into two inboard (IB) and outboard (OB) sections with the IB section being nearest radially to the central solenoid of the tokamak's magnetic coils. A visual cross section of the ARC-2018 design from a CAD drawing is included in Figure 1.3.1. In this figure, the major components as modeled in the MELCOR/TMAP input file are shown. Each colored section represents a different section which is then further subdivided into multiple CVs and HSs in the input file for a finer nodal resolution.

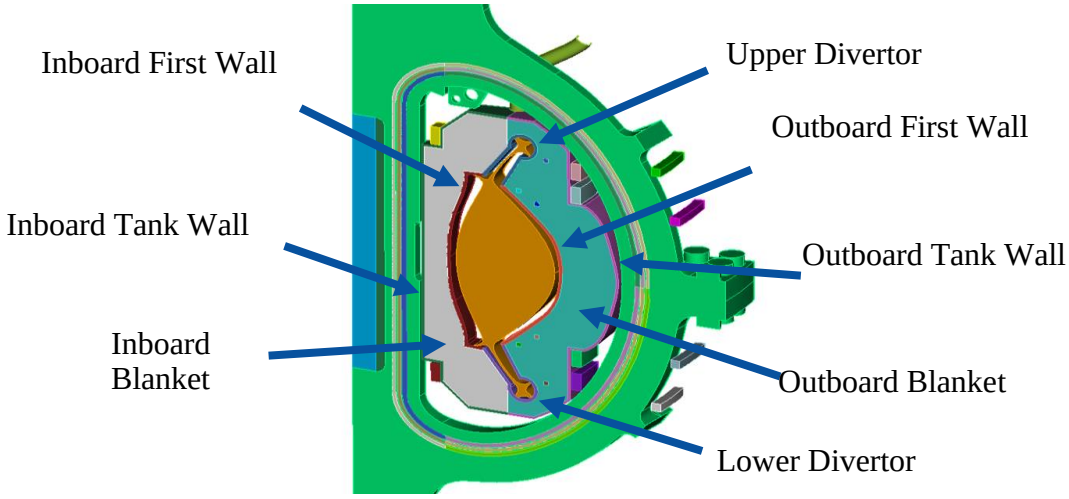

Figure 1.3.1. Layout of major components of the ARC-2018 device as defined in the MELCOR/TMAP input file.

Figure 1.3.2 displays the radial placement and thicknesses of the double wall vacuum vessel based on the ARC-2018 device design as implemented in the MELCOR-TMAP input file. Extending from the plasma and moving outward radially, the plasma-facing surface is the first wall (FW) composed of tungsten which is separated into three layers with thicknesses of 0.01 microns, 10 microns, and 1 mm. These different tungsten layers have identical material properties in the MELCOR/TMAP input file except for differing trap densities. Extending beyond the FW in the radial direction, the inner vacuum vessel (VV) wall composed of Inconel-718 nickel alloy is followed by the FLiBe coolant channel, a beryllium multiplier, and the outer VV. The outer VV is then connected to the FLiBe blanket volume contained in the outer immersion tank. As for the boundary conditions, within the HSs for the inner VV wall, the tritium source is limited to the 0.01-micron layer immediately facing the plasma. These choices follow the ARC 2018 [20] paper. It should be noted that the ARC radial build and material selection is not finalized and is continuing to be studied at CFS.

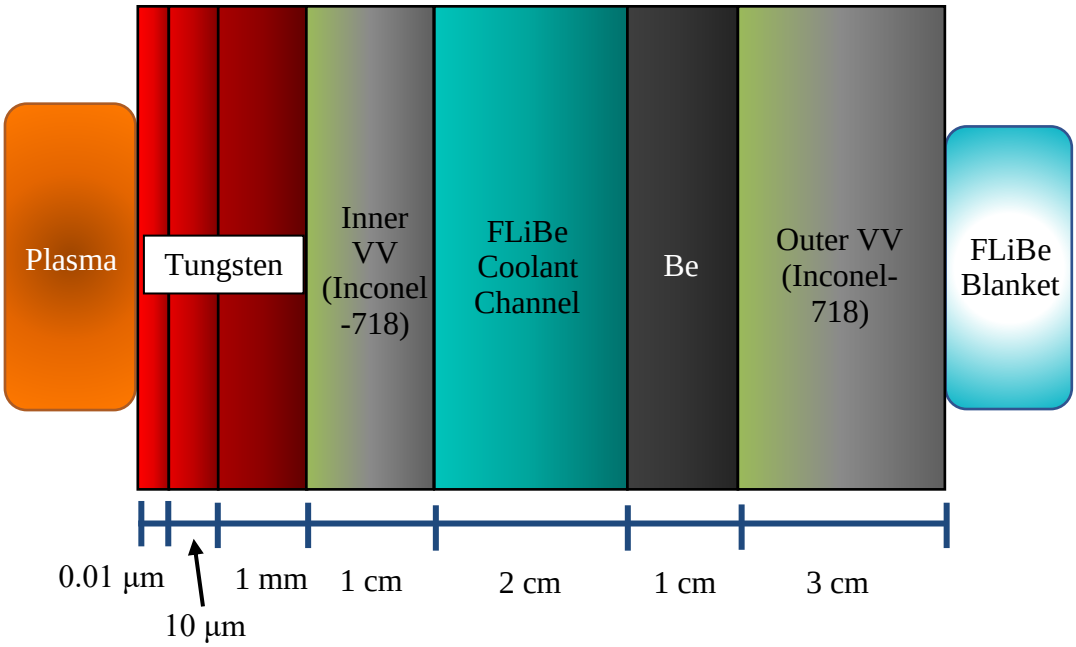

Figure 1.3.2. Radial layers of double wall vacuum vessel based on ARC-2018 as implemented in MELCOR/TMAP input file. Layer thicknesses are not to scale.

Flow paths are an integral component of the MELCOR/TMAP input file. These control the transfer of a fluid (single or multiphase) and any hydrogen species contained within that fluid from one CV to another. The flow path connections between the FLiBe source and other CVs in the MELCOR/TMAP model of the ARC-2018 design are represented in Figure 1.3.3. Figure 1.3.3 shows the flow paths that connect the manifold to the inboard and outboard coolant channels and inboard blanket, as well as to an expansion tank. The outboard blanket also connects to the heat exchanger and tritium extraction system via the hot leg. The hot leg connects to the tritium extraction CV, extraction outlet, HX, and cold leg which loops back to the manifold CV as described in the MELCOR/TMAP input file. For these figures, each arrow represents a flow path where FLiBe (and tritium, when present) with the arrow pointing from the source CV and to the destination CV. The coolant channels for the IB VV wall and lower divertor OB leg connect to the IB blanket CV, and the OB VV wall and upper divertor IB leg coolant channels connect to the OB blanket CV. There is also the exchange of FLiBe through flow paths between the IB and OB blankets at the lower and upper edges of the blanket.

Following the hot leg CV, a flow path transfers FLiBe to the tritium extraction and HX systems. The FLiBe transporting the tritium passes through the tritium extraction system with a fixed percentage of its tritium removed from the volume; the default value for the base case is 90%. This value is modified for the study to follow which determines the effects caused by affecting this tritium extraction system efficiency. The stream exiting the tritium extraction system merges with that which bypassed the system at the Extraction Outlet CV. This continues to the HX system which is subdivided into 10 different sections. Tritium and heat transfer through individual HSs for each section to a sink specifically designed for the HX system, the HX Sink CV (not shown in the figure). The reason for this subdivision of CVs is to increase the nodal resolution for tritium and heat extraction from the FLiBe. The HX system then transfers FLiBe to the cold leg CV and finally to the manifold CV before returning to the device.

The manifold CV behaves similarly to a plenum which collects FLiBe that has passed through the VV coolant channels and the tritium extraction and HX systems. The FLiBe in the manifold CV is then recirculated to various CVs throughout the device including the IB blanket, IB and OB coolant channels, lower and upper divertor coolant channels, and the Sink CV as shown in Figure 1.3.3. The expansion tank CV is a large volume (100.0 m^3) in the model which serves as a containment tank for excess FLiBe. For the simulations reported here, the expansion tank is a time-independent control volume to aid in stabilizing the hydrodynamics of the simulation at initialization. Simulations were also performed where the flow was severed to this expansion tank after reaching a steady-state permeation in all components following 8 weeks of simulation time. These latter simulations with the closed connection to the expansion tank resulted in a negligible difference in tritium inventory and permeation as a function of time. Thus, the final results in this report are considered to not have been affected by the existence of this expansion tank in the model.

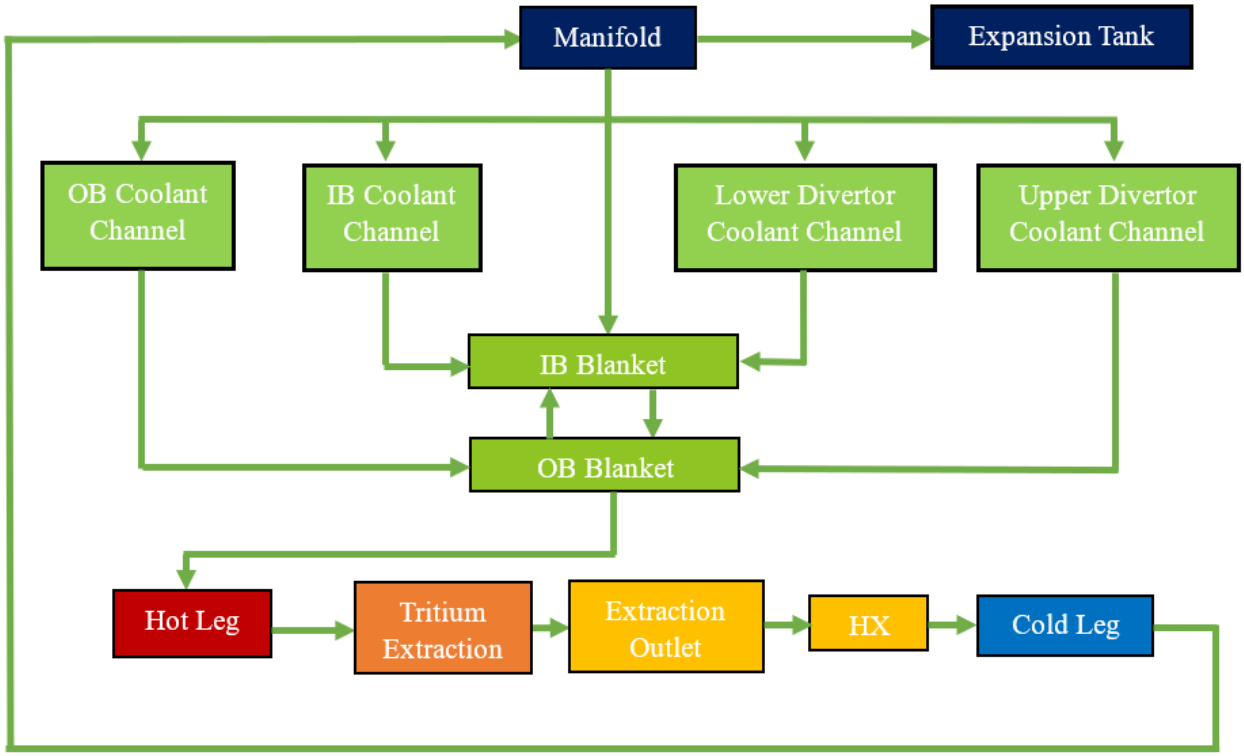

Figure 1.3.3. Flow path connections for transportation of FLiBe from the manifold throughout the coolant and blanket channels and through the tritium extraction and heat exchanger (HX) system which reconnects to the manifold. An expansion tank is also connected to the manifold.

1.3.2 Results of Steady-State Tritium Transport Analysis

Two key output parameters from the MELCOR/TMAP simulations are tritium permeation through solid structure materials to external containment as well as the mobile and diffused inventory of

tritium within the structural materials. External containment for an ARC-class power plant may include an intermediate salt loop, secondary tritium cleanup systems, etc. The following two figures and two tables display the tritium permeation rate in grams/year and tritium inventory in grams, respectively, using MELCOR/TMAP for the base case up to one year of simulation time (which corresponds to approximately one full year of ARC operation starting from cold startup conditions). Figure 1.3.5 and Figure 1.3.6 show the time-dependent tritium permeation rate and inventory up to one year of simulation time, respectively, and Table 1.3.4 and Table 1.3.5 report the final values of tritium permeation rate and inventory at one year of simulation time, respectively. Subsequent tables and figures will be compared to these values for comparison. For the purposes of this calculation, the HX is assumed to be coated with 0.1 mm of tungsten using the material properties described in Table 1.3.2 and trap energies in Table 1.3.3. The permeation calculation results for the base case demonstrate that permeation rates are largest across the outer FLiBe immersion tank walls, representing approximately 76% of the total tritium permeation rate. As for the inventory calculation results, the plasma-facing FWs located at the divertors have the highest tritium inventory, holding approximately 70% of the total inventory. Compared to the combined inventory at the inboard and outboard plasma-facing FWs and inner VV with ~23 g of tritium, the divertor FWs have over six times this inventory.

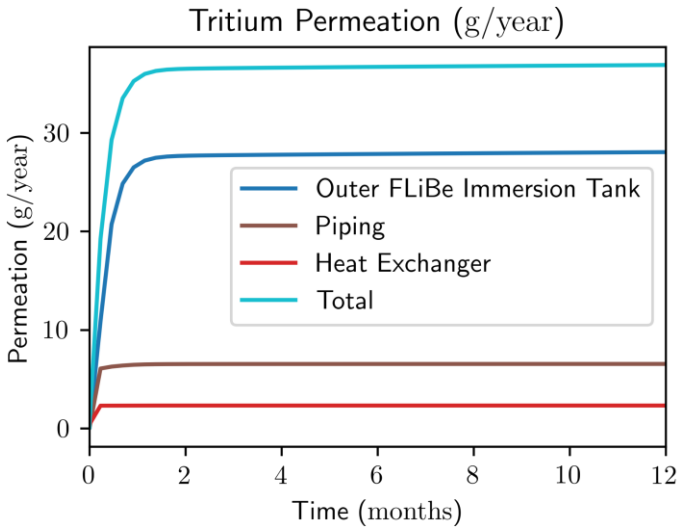

Figure 1.3.5. Tritium permeation to external containment in ARC-2018 model in grams per year versus time for up to one year of projected ARC-2018 operation time.

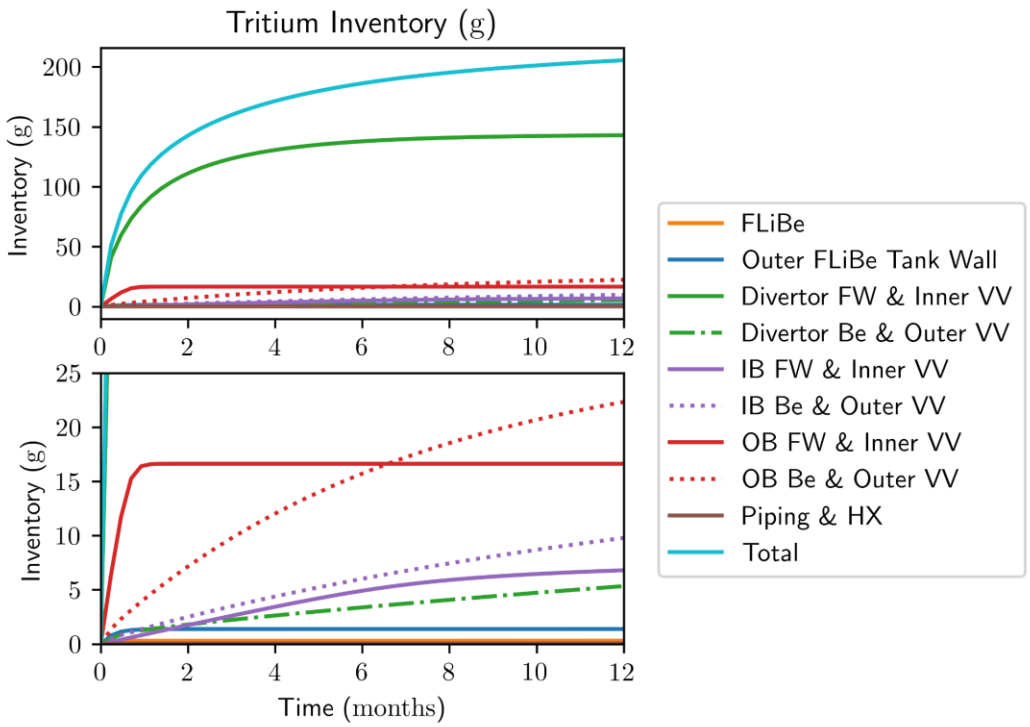

Figure 1.3.6. Tritium inventory from ARC-2018 model in grams versus time up to one year of projected ARC-2018 operation time. Reductions in inventory can be achieved with further design optimization and R&D work.

Table 1.3.4. Tritium permeation rate across major components of ARC-2018 model after one year of projected ARC-2018 operation time.

Permeation Rate Location	**Location Label**	**Tritium Permeation Rate (g/year)**	**Percent of Total Permeation Rate (%)**
Outer FLiBe Immersion Tank Wall	1	28.04	76.0
Pipes	2	6.53	17.7
Heat Exchanger w/ 100 um W permeation barrier	3	2.31	6.3
Total	4	36.88	100.0

Table 1.3.5. Tritium inventory in major components of ARC-2018 model after one year of projected ARC-2018 operation time.

Inventory Location	**Location Label**	**Tritium Inventory (g)**	**Percent of Total Inventory (%)**
FLiBe in Coolant & Blankets	1	0.30	0.1
Outer FLiBe Tank Wall	2	1.39	0.7
FW & Inner VV for Upper & Lower Divertors	3	142.97	69.6

Be Multiplier and Outer VV for Upper & Lower Divertors	4	5.33	2.6
IB FW & Inner VV	5	6.80	3.3
IB Be Multiplier & Outer VV	6	9.76	4.8
OB FW & Inner VV	7	16.63	8.1
OB Be Multiplier & Outer VV	8	22.31	10.8
Piping & HX Systems	9	0.07	< 0.1
Total	10	205.55	100.0

The results of the study of tritium permeation rate and inventory as a function of the efficiency of the tritium extraction system efficiency are summarized in Tables 1.3.6 and 1.3.7 and Figures 1.3.7 and 1.3.8. For these tables and figures, the results are subdivided between major components of the device using the same inventory and permeation rate labels as from Tables 1.3.4 and 1.3.5. Tables 1.3.6 and 1.3.7, respectively, give the projected permeation rates and inventory, respectively, for the base case with varying tritium extraction efficiency values with the base case at 90% tritium extraction efficiency (default value) being highlighted. The permeation rate labels and inventory labels in Tables 1.3.6 and 1.3.7 are the same as those from Tables 1.3.4 and 1.3.5, respectively.

Examining Table 1.3.6, the permeation rates most affected by the varying tritium extraction efficiencies are those from the HX system (Permeation Rate Label 3); this is to be expected as the tritium extraction system immediately precedes the HX system in the FLiBe coolant flow loop. As tritium extraction system efficiency increases, less tritium remains in the FLiBe to permeate through the HX system walls. Thus, approaching 99.99% extraction efficiency, the permeation rate through the HX system drastically reduces by 97.4% compared to the base case's 90% extraction efficiency (from over 2 grams per year for the base case to less than 0.1 gram per year). By comparison, the permeation rate through the pipes (Permeation Rate Label 2) has a reduction in permeation rate of 14.2% from the Base Case of 90% extraction efficiency to the 99.99% extraction efficiency case (from 6.53 to 5.6 grams per year). Finally, in terms of percentage difference from the Base Case, the outer FLiBe tank wall (Permeation Rate Label 1) is least affected by the tritium extraction system efficiency; increasing the extraction system efficiency from 90% to 99.99% only reduces the tritium permeation rates by 7.3% (from 28.04 to 25.98 grams per year). However, this is still a larger raw tritium permeation rate difference as compared to that for the piping system (2.06 grams per year difference from the tank wall versus 0.93 grams per year difference from the piping system). This data is valuable for the future design of the tritium extraction system and in determining the locations of the highest permeation rates such that design decisions (e.g., consideration of wall thicknesses and materials) can be made to minimize tritium those rates.

Considering the inventory of tritium after 1 year of simulation time in Table 1.3.7, the results show that there is a minimal change in inventory as a function of tritium extraction system efficiency. Between the Base Case efficiency of 90% and the case with 99.99% efficiency, the difference in total inventory (inventory location 10), the difference is only 0.90% (from 205.55 grams to 203.71 grams). In the case of the FW and inner VV of the upper and lower divertors (inventory location 3), though it represents the highest source of tritium inventory at 142.97 grams for the Base Case, it remains relatively unchanged as a function of tritium extraction system efficiency (less than 0.02

grams difference). Since the divertor components are connected to the sources of the tritium (from both the Source volume, see Figure 1.3.3, and the tritium sources at the FW) and are at the opposite end of the FLiBe coolant loop as compared to the HX system, it follows the expectation that this inventory value would be unaffected by changes to the tritium extraction system efficiency.

Figures 1.3.7 and 1.3.8 show the tritium permeation rate through the HX system as a function of tritium extraction system efficiency. In these figures, the value of 100% on the y-axis represents the tritium permeation across the heat exchanger as calculated in the base case with a tritium extraction efficiency of 90%. The results show a non-linear relationship between tritium permeation across the heat exchanger and the tritium extraction efficiency for all material settings for tritium permeation. This data shows the calculated tritium permeation rate from the HX system as a function of the tritium extraction efficiency as set in the MELCOR/TMAP input. As the tritium extraction system immediately precedes the HX system in the FLiBe coolant loop (see Figure 1.3.3), it is expected that the permeation rate through the HX system would decrease with increasing tritium extraction efficiency. These two figures confirm this expectation.

Figure 1.3.7 shows the tritium permeation rate through the HX system for the Base Case as compared to two cases: the first where the FLiBe solubility values are changed from those provided by that of Nakamura et al. [1] to those from Calderoni et al. [2] (labeled, "FLiBe Properties from Calderoni et al., 2008"), and the second where the FLiBe diffusivity values are changed from those of Calderoni et al. to Nakamura et al (labeled, "FLiBe Properties from Nakamura et al., 2015"). In these cases, the solubility and diffusivity values for FLiBe are solely from Calderoni et al. and Nakamura et al., respectively, rather than being mixed values as in the Base Case (i.e., solubility from Nakamura et al., diffusivity from Calderoni et al.). This compares the effect due to the change in FLiBe solubility or diffusivity from the Base Case values. As the curve for the Nakamura et al. data demonstrates, changing the diffusivity from Calderoni et al. in the Base Case to Nakamura et al. produced only a marginal difference in permeation rate across the HX system (less than 1 percent difference). By comparison, the change of the Base Case solubility parameters to those from Calderoni et al. resulted in a decrease in permeation from the HX system (ranging between 29.3% to 30.5% reduction). This demonstrates that the permeation rate of tritium across the HX system is far more sensitive to the FLiBe diffusivity than solubility.

In Figure 1.3.8, the base case is compared to a modified input which changed the base case's tritium transport properties for tungsten to those from Esteban et al. [15]; as shown in Figure 1.2.3 and Figure 1.2.4, respectively, Esteban et al. reported significantly higher solubilities at temperatures below 1000 K and lower diffusivities (with a difference by three orders of magnitude) for hydrogen in tungsten as compared to Frauenfelder et al [4]. Considering Figure 1.3.8, the change in permeation through the HX system increases drastically when changing properties to those provided by Esteban et al. (an increase ranging from 759% to 6,733%). This may be explained by the solubilities reported by Esteban et al. in the range of 800 K to 1000 K are nearly three orders of magnitude higher than those reported by Frauenfelder. As the results show by changing the FLiBe solubilities and diffusivities, it appears that solubility in both the FLiBe and tungsten have a significant effect on the permeation of tritium through the HX system. The high degree of variance in the reported transport values in tungsten means further study may be needed to better quantify these values.

The effect of tungsten properties on permeation are further explored in the study of modifying the thickness of a tungsten lining of the HX system that follows. As shown in the results in the

preceding paragraphs, the amount of tritium that permeates through the HX system is more sensitive to the efficiency of the tritium extraction system, tungsten properties, and FLiBe solubility than the FLiBe diffusivity used in the Base Case model.

Table 1.3.6. Permeation rate (grams/year) of tritium to external containment after one year of projected ARC-2018 operation time assuming varied tritium extraction efficiencies from the base case of 90% efficiency (highlighted). Permeation Rate Source Label descriptions are given in Table 1.3.4.

Efficiency (%)	**Permeation Rate Source Label**			
	1	**2**	**3**	**4**
10	110.98	69.33	20.77	201.08
30	58.68	24.09	10.59	93.36
50	41.43	13.79	6.94	62.16
70	33.21	9.17	4.54	46.92
90 (Base Case)	28.04	6.53	2.31	36.88
95	28.14	6.04	1.59	35.77
97.5	27.65	5.81	1.11	34.57
99.75	26.03	5.62	0.34	31.99
99.99	25.98	5.60	0.06	31.64

Table 1.3.7. Inventory (grams) of tritium after one year of projected ARC-2018 operation time assuming varied tritium extraction efficiencies modified from the base case of 90% efficiency (highlighted). Inventory Label descriptions are given in Table 1.3.5.

Efficiency (%)	**Inventory Label**									
	1	**2**	**3**	**4**	**5**	**6**	**7**	**8**	**9**	**10**
10	3.09	4.96	142.96	10.74	10.20	12.26	18.76	26.68	0.49	230.13
30	1.00	2.71	142.96	7.46	9.27	10.71	17.40	23.93	0.21	215.65
50	0.58	2.00	142.97	6.42	8.70	10.25	16.97	23.13	0.14	211.14
70	0.40	1.62	142.97	5.79	8.17	9.97	16.76	22.64	0.10	208.43
90 (Base Case)	0.30	1.39	142.97	5.33	6.80	9.76	16.63	22.31	0.07	205.55
95	0.29	1.36	142.96	5.21	6.23	9.69	16.60	22.19	0.06	204.58
97.5	0.28	1.34	142.96	5.15	5.91	9.67	16.59	22.15	0.05	204.11
99.75	0.27	1.30	142.97	5.11	5.61	9.69	16.58	22.19	0.05	203.76
99.99	0.27	1.29	142.97	5.11	5.57	9.69	16.58	22.18	0.04	203.71

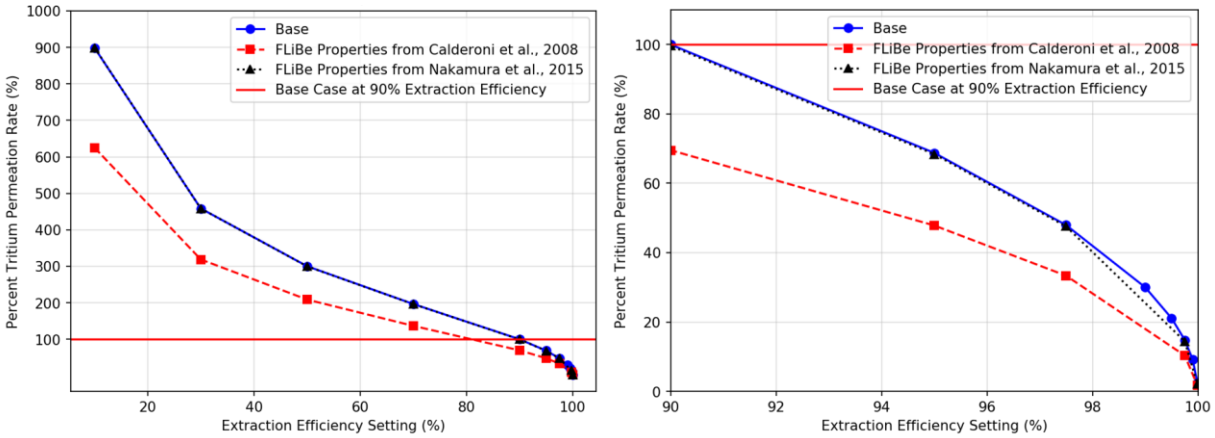

Figure 1.3.7. Tritium permeation rate across the HX system to external containment compared to the base case as a function of the efficiency of the tritium extraction system with differing FLiBe diffusivities and solubilities.

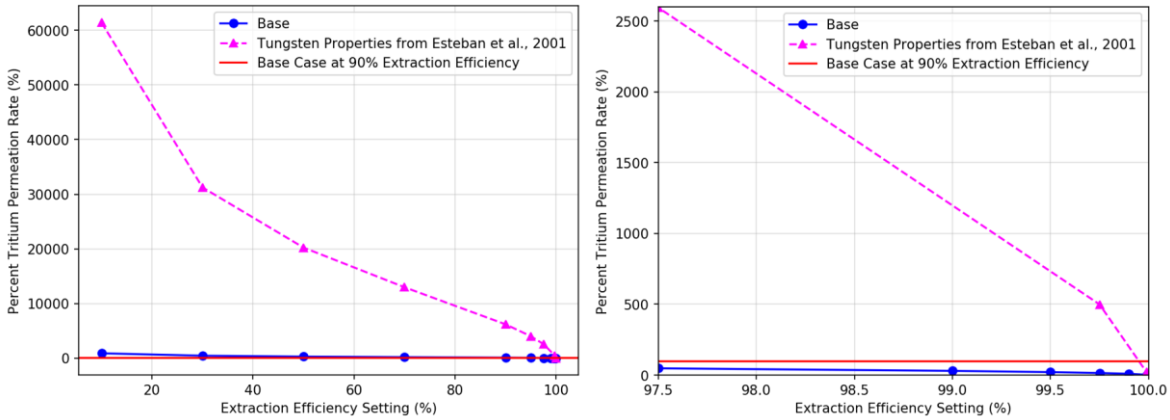

Figure 1.3.8. Tritium permeation rate across the HX system to external containment compared to the base case as a function of efficiency of the tritium extraction system with differing tungsten properties.

Table 1.3.8 compares the concentration of tritium in the Hot Leg CV (before tritium is extracted) to the Extraction Outlet CV (after tritium is extracted) as a function of the tritium extraction system efficiency after one year of projected ARC-2018 operation. The second and third columns provide the calculated concentration values from the MELCOR-TMAP simulations, the fourth column is the difference between the second and third columns, the fifth column is the percent difference (taking the fourth column and dividing by the second column), and the sixth column is the percent difference in concentration as compared to the 90% tritium extraction efficiency (base case). As expected, with increasing tritium extraction efficiency, concentration drop from the FLiBe loop by passing through the tritium extraction system increases based on the summary in the fourth column. However, this increase in tritium extraction efficiency results in a decrease in the concentration of the Hot Leg CV prior to extraction. More will be discussed on the implications of these results. The percentage of tritium extracted from the FLiBe as listed in column five equals the tritium extraction efficiency setting (column one) to the fourth significant figure in every case; this confirms that the tritium extraction system within the MELCOR-TMAP input file functions as designed. The sixth column is useful for showing how much concentration change difference

results by modifying the tritium extraction system efficiency from the Base Case. As stated previously, a change in this extraction efficiency results in a modified tritium concentration in the Hot Leg CV. Since the tritium extraction efficiency is based on the concentration of tritium in the Hot Leg CV, a decrease in the Hot Leg CV tritium concentration results in a decrease in the total amount of extracted tritium per percent extraction efficiency. In other words, this results in diminishing returns; an increase in tritium extraction efficiency results in a decrease in tritium concentration prior to extraction. In such a case, the total quantity of tritium extracted is increased by a diminishing percentage as tritium extraction efficiency is increased. For example, a change in extraction efficiency from 90 to 95 percent – a 5 percent increase in extraction efficiency – results in a 0.0038 percent increase in extracted concentration of tritium. Increasing the tritium extraction system efficiency by a further 4.99 percent to a value of 99.99 percent increases the extracted tritium by 0.0129 percent to a total of 0.0167 percent compared to the 95 percent extraction efficiency case. This information is useful when designing the tritium extraction system to determine the desired extracted tritium from the FLiBe loop as well as to determine the economics of tritium extraction efficiency.

Table 1.3.8. Change in tritium concentration in the FLiBe loop as a function of the tritium extraction system efficiency.

	Concentration of Tritium (atoms/m^3)				
One-pass Extraction Efficiency (%)	**Hot Leg CV,** $C_{T,HL}$	**Extraction Outlet CV,** $C_{T,EO}$	**Difference,** $\Delta C_{T,i} = C_{T,HL} - C_{T,EO}$	**Percent Difference,** $100\left(\frac{\Delta C_{T,i}}{C_{T,HL}}\right)$	**Percent Difference from Base Case at 90%,** $100\left(\frac{\Delta C_{T,i} - \Delta C_{T,90\%}}{\Delta C_{T,90\%}}\right)$
10	$7.739(10^{20})$	$6.965(10^{20})$	$7.738(10^{19})$	10.00	-0.594
30	$2.590(10^{20})$	$1.813(10^{20})$	$7.769(10^{19})$	30.00	-0.2
50	$1.556(10^{20})$	$7.778(10^{19})$	$7.778(10^{19})$	50.00	-0.087
70	$1.112(10^{20})$	$3.335(10^{19})$	$7.782(10^{19})$	70.00	-0.0317
90 (Base Case)	$8.649(10^{19})$	$8.647(10^{18})$	$7.785(10^{19})$	90.00	0.000
95	$8.194(10^{19})$	$4.095(10^{18})$	$7.785(10^{19})$	95.00	0.00382
97.5	$7.985(10^{19})$	$1.994(10^{18})$	$7.785(10^{19})$	97.50	0.00774
99.75	$7.805(10^{19})$	$1.931(10^{17})$	$7.786(10^{19})$	99.75	0.0155
99.99	$7.787(10^{19})$	$5.788(10^{15})$	$7.786(10^{19})$	99.99	0.0167

In order to study the effect of tungsten in tritium retention in the HX system, test cases were made to replace varying thicknesses of the Inconel-718 material in the HX system on the FLiBe-facing side with tungsten. The chosen tungsten thicknesses were 0.001 mm, 0.01 mm, and 0.1 mm. Using the base case tritium extraction efficiency of 90%, these simulations were run using both the base case tungsten material properties and those from Esteban et al. [15] for comparison. The results of this study are included in Figure 1.3.9. Note that the y-axis represents the tritium permeation rate in grams per year, and the x-axis represents the tungsten layer thickness in the HX system in millimeters. As the x-axis is in logarithmic format, the setting for zero tungsten thickness was set to 10^{-4} mm. The results demonstrate that replacing even a micron (0.001 mm) of the innermost layer of Inconel-718 had a large effect on the tritium permeation through the HX system according

to the base case material settings, reducing the tritium permeation rates by approximately 73%. However, using the tungsten diffusivities from Esteban et al. resulted in only approximately 1% reduction in tritium permeation when using a 0.001 mm-thick tungsten layer. A 0.01 mm-thick layer (10 microns) reduced the tritium permeation rate from the base case by 97% using the base case material settings and by approximately 21% using the Esteban et al. tungsten parameters. Finally, a 0.1 mm-thick layer (100 microns) of tungsten reduced the tritium permeation rate by over 99% for the base case.

These results indicate that adding a tungsten layer to the HX system can have a dramatic effect on tritium permeation rates (up to potentially 97%), even if that layer is only 10 microns thick. Note that these results are for exploring an idealized case where the tungsten layer is of an equal thickness in the pipes with no variation and has a perfect and uniform adherence to the Inconel-718 layer with no additional resistance between the layers. In a real-world HX system, there may be imperfections due to cracks and microfractures, microscopic gaps between the tungsten and Inconel-718 layers, or other conditions that would affect the transport of tritium through the HX pipes. Also, any thermal expansion due to change in device operating temperature is not accounted for in this study; as the device increases in temperature following startup, reaching steady state, and cooling down following shutdown, the tungsten film thicknesses and transport properties would be expected to change accordingly. Imperfections in the tungsten layer would likely increase tritium permeation through it. These effects may be worth investigating in the future.

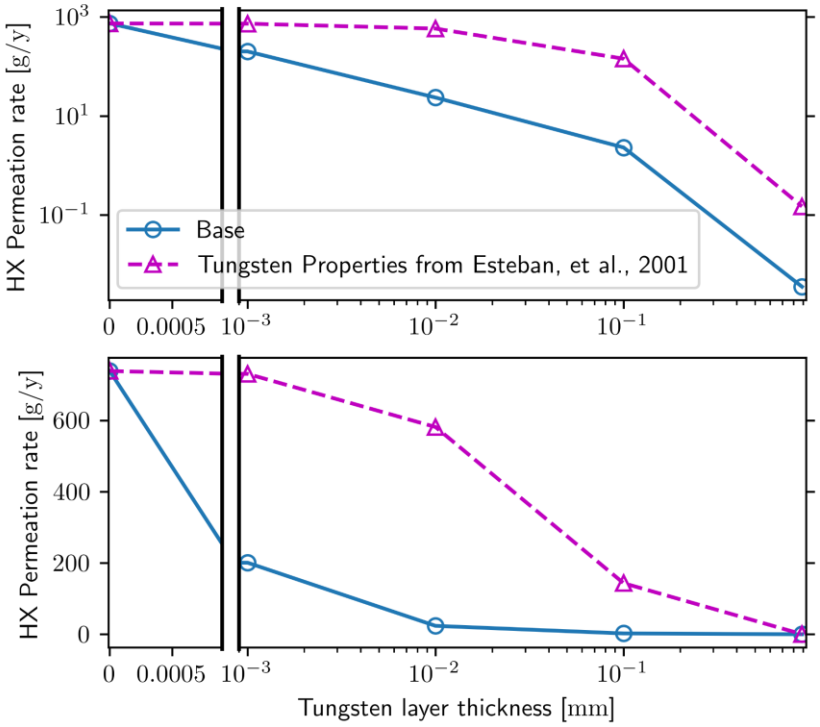

Figure 1.3.9. Tritium permeation rate from HX system as a function of tungsten layer thickness on the FLiBe-facing surface of the HX system (shown log-log above and semilog below).

The tritium permeation rates and inventories are compared in the following figures. Summarized in Figures 1.3.10 and 1.3.11 are the differences in tritium permeation rates and inventories, respectively, from the base case due to change in FLiBe solubilities and diffusivities. Similarly, Figures 1.3.12 and 1.3.13 show the differences in tritium permeation rates and inventories, respectively, from the base case due to change in tungsten material properties from the base case by Frauenfelder to Esteban et al. [15]. As in previous figures, the permeation rate label descriptions in Figures 1.3.10 and 1.3.12 are provided in Table 1.3.4 and the inventory label descriptions in Figures 1.3.11 and 1.3.13 are found in Table 1.3.5. In Figures 1.3.10 and 1.3.11, considering parameter changes for FLiBe only, the following bar labels are associated with the accompanying datasets: "Calderoni" with solubility and diffusivity parameters from Calderoni et al. [2]; "Nakamura" with solubility and diffusivity parameters from Nakamura et al. [1]; "Malinauskas & Calderoni Diffusivity" with solubility from Malinauskas & Richardson [16] and diffusivity from Calderoni et al.; "Malinauskas & Nakamura Diffusivity" with solubility from Malinauskas & Richardson and diffusivity from Nakamura et al.

Figure 1.3.10 shows that the most significant difference in tritium permeation rate from the HX system (permeation location 3) is due to the change in solubilities from the base case from those of Nakamura et al. to those from Malinauskas et al. The "Malinauskas & Calderoni" and "Malinauskas & Nakamura" data (which both use FLiBe solubility from Malinauskas & Richardson) show an increase by 61.6 grams/year (167.0% of the total base case permeation) and 54.15 grams/year (146.8% of the total base case permeation), respectively, from the base case. By contrast, changing the solubility to that from Calderoni et al. (as shown in the "Calderoni" data) results in a difference of -0.70 grams (-1.91% of the total base case permeation) at this location. The permeation from the outer FLiBe immersion tank wall (permeation location 1) are most affected by the change from solubility to that of Malinauskas & Richardson; the "Malinauskas & Calderoni" data show a difference in 33.8 grams/year (91.7% of the total base case permeation). Changing the diffusivity from the base case to create the "Nakamura" data resulted in a -4.69 gram/year (-40.9% of the total base case permeation) permeation from the FLiBe outer tank wall. This demonstrates that, for this inventory location, both the solubility and diffusivity have an appreciable impact on permeation. The piping systems (permeation location 2) has a lower impact due to changing either solubility or diffusivity, with a maximum of 4.7 grams/year permeation (12.7% of the total base case permeation) difference from the base case by both cases which use diffusivity parameters from Nakamura et al. ("Nakamura" and "Malinauskas & Nakamura" data). The remaining cases which use diffusivity parameters from Calderoni et al., the "Calderoni" and "Malinauskas & Calderoni" data differ from the base case by -0.20 grams/year (-0.55% of the total base case permeation) and 1.11 grams/year (3.02% of the total base case permeation), respectively. This shows a higher sensitivity in permeation at this location due to change in diffusivity than that of solubility.

The results presented in Figure 1.3.11 shows that the tritium inventory is more dependent on the inventory location and set of FLiBe data than is the case with the tritium permeation rates in the prior figure. Considering all the data sets, the tritium inventories in the FLiBe (including coolant channels and blankets), outer FLiBe immersion tank wall, upper and lower divertor FW and inner VV, and the HX and piping systems (inventory locations 1, 2, 3, and 9) have a lower sensitivity to FLiBe solubility and diffusivity values. This is evident by the less than ±2.0-gram difference in

tritium inventory in these four inventory locations from the base case for all FLiBe datasets. The quantities of tritium in those components are reasonably unaffected when varying FLiBe diffusivity and solubility values across the four datasets used in this study. Thus, they are not considered to be major contributors to the overall difference in tritium inventory due to change in FLiBe properties. This is expected in the cases of inventory locations 1, 2, and 9 as they were relatively minor contributions in the base case to the overall total tritium inventory according to the results given in Table 1.3.5, contributing only 0.15%, 0.68%, and 0.03% to the total tritium inventory, respectively. However, the FW and inner VV for the upper and lower divertors (inventory location 3) had the largest contribution in the base case to the overall tritium inventory of any of the inventory locations at 142.98 grams or 69.5% of the total inventory. The change in inventory at this location is on the order of 1 milligram, or about 5 orders of magnitude lower than the tritium inventory; thus, the sensitivity of the FW and inner VV tritium inventory in the divertors to FLiBe solubility and diffusivity is so small as to be negligible for all FLiBe property datasets. This may be explained due to the existence of a high tritium flux at the FW for the divertors; since the FW and inner VV are radially nearest to the plasma, they are relatively unaffected by the change in the properties of the FLiBe which are farther extending radially outward from the FW and inner VV. However, the difference in tritium inventory due to a change in FLiBe properties are expected to be larger for those areas radially farther outward from the FLiBe coolant channel (including the Be multiplier, outer VV, and blanket). This expectation is evaluated when addressing the results for other inventory locations to follow.

Continuing to examine the results in Figure 1.3.11, the inventory locations that are more highly dependent on FLiBe solubility and diffusivity are the Be multiplier and outer VV for the upper and lower divertors, inboard first wall and inner VV, inboard Be multiplier and outer VV, outboard FW and inner VV, and outboard Be multiplier and outer VV (inventory locations 4, 5, 6, 7, and 8, respectively). These are the major contributors to the total change in tritium inventory due to change in FLiBe solubility and diffusivity. As described previously, it was expected that the inventory differences would be larger for the Be multiplier and outer VV for the upper and lower divertors (inventory location 4) as compared to the FW and inner VV of the divertors (inventory location 3); examining the inventory location 4 results for the cases using FLiBe solubilities from Malinauskas & Richardson, the “Malinauskas & Calderoni Diffusivity” dataset shows a 26.9 gram or 13.1% difference from the base case total inventory, while the “Malinauskas & Nakamura Diffusivity” dataset shows a 8.88 gram or 4.32% difference from the base case total inventory. This agrees with the expectation that there would be a larger difference in tritium inventory beyond the FLiBe coolant channel. However, the “Calderoni” and “Nakamura” cases at the same location show an insignificant change (with changes of -0.28 grams or -0.13% of the base case total and less than 0.01 grams or 0.33% of the base case total, respectively). It appears that the change in 2 to 3 orders of magnitude for the solubility in FLiBe from the data provided by Malinauskas & Richardson compared to those from Nakamura et al. and Calderoni et al., respectively, has a much higher change in inventory than by changing the diffusivity by 1 order of magnitude from Calderoni et al. to Nakamura et al. The significantly lower solubility may result in a larger buildup of tritium in the solid structural materials rather than remaining dissolved in the FLiBe, hence the higher inventory for those cases using the Malinauskas & Richardson solubilities. This will also be shown to be the case for other inventory locations.

Among the inventory changes shown in Figure 1.3.11, the lowest changes from the base case are found in the tritium inventory in the inboard FW and inner VV (inventory location 5). Each of the FLiBe datasets differs from the base case within ±3.8 grams of the base case, which represents

about 1.83% of the total base case inventory. This is a non-negligible change in tritium inventory at this location, but it does not represent a large percentage of the total inventory quantity. The reason for the relatively small change may reflect the inventory at the FW and inner VV for the divertors; since there is a relatively high flux at the FW and the FLiBe exists farther out from the flux source, the change in FLiBe properties wouldn't result in a large change in inventory at the FW and inner VV. The region beyond the inboard inner VV and FLiBe channel at the Be multiplier and outer VV (inventory location 6) does demonstrate a markedly larger difference in tritium inventory for the two cases using solubility from Malinauskas & Richardson (21.3 grams or 10.3% of the base case total for the "Malinauskas & Calderoni Diffusivity" dataset and 11.1 grams or 5.40% of the base case total for the "Malinauskas & Nakamura Diffusivity" case), while those using solubilities from Nakamura et al. and Calderoni et al. are relatively unaffected (with changes of -0.21 grams or -0.10% of the base case total for the "Calderoni" dataset and 0.23 grams or 0.11% of the base case total for the "Nakamura" dataset). As described for the case of inventory location 4, the significantly lower solubility from Malinauskas & Richardson proves to have a significant effect on inventory over and above the difference between the solubilities from Calderoni et al. and Nakamura et al., most likely due to the lower maximum concentration of tritium allowed in the FLiBe, resulting in an increased concentration within the solid structures.

The OB FW and inner VV (inventory location 7) and OB Be multiplier and outer VV (inventory location 8) show a similar relationship described previously between the FW and inner VV and Be multiplier and outer VV for the upper and lower divertors (inventory locations 3 and 4, respectively) or that of the IB FW and inner VV and IB Be multiplier and outer VV (inventory locations 5 and 6, respectively). This relationship is that the walls located closer to the plasma demonstrate a markedly lower change in tritium inventory due to change in material properties from the base case than at locations radially farther beyond the FLiBe coolant channel. It is also shown that the greatest change is again related to changing the solubility to that of Malinauskas & Richardson. There is an increase of 13.9 grams (6.74% of the total inventory) and 15.4 grams (7.49% of the total inventory) of tritium when changing the FLiBe solubility to that of Malinauskas & Richardson from Nakamura et al. in the OB FW and inner VV (inventory location 7) and the diffusivity to that of Calderoni et al. and Nakamura et al., respectively. Notably, the change is much more significant in the OB Be multiplier and outer VV (inventory location 8), having an increase in tritium inventory by 48.9 grams (23.7% of the total inventory) and 35.5 grams (17.3% of the total inventory) using Malinauskas & Richardson and diffusivities from Calderoni et al. and Nakamura et al., respectively. This could be similarly explained as previously that the change in FLiBe properties is more highly dependent at the Be multiplier and outer VV due to being located farther from the tritium sources at the plasma-facing walls where the flux is highest as described with the previous inventories. The results also show that a larger change occurs when using the FLiBe diffusivities from Calderoni et al. as compared to those from Nakamura et al. in combination with solubilities from Malinauskas & Richardson (48.9 grams versus 35.5 grams, respectively) at the OB Be multiplier and outer VV, though the changes are comparable at the OB FW and inner VV (13.9 grams versus 15.4 grams, respectively.

When examining the combined change in tritium inventory across all inventory locations due to a change in FLiBe tritium transport properties (inventory location 10), there are relatively negligible changes in inventory by only changing the base case's solubilities to those from Calderoni et. al (-3.28 grams or -1.60% of the total inventory) or only the diffusivity to that of Nakamura et al. (-1.23 grams or -0.60% of the total inventory). The greatest changes are those which change the base case solubility to that of Malinauskas & Richardson; with the base case's FLiBe diffusivities from

Calderoni et al., the change in solubility results in a 115.0-gram increase in tritium inventory (55.9% of the total inventory), while changing the diffusivities to those from Nakamura et al. results in an increase of 66.5 grams (32.4% of the total inventory). This demonstrates that, with the available FLiBe datasets, the diffusivity changes are not so important on their own unless combined with the change in solubilities from those of Calderoni et al. or Nakamura et al. to those from Malinauskas & Richardson.

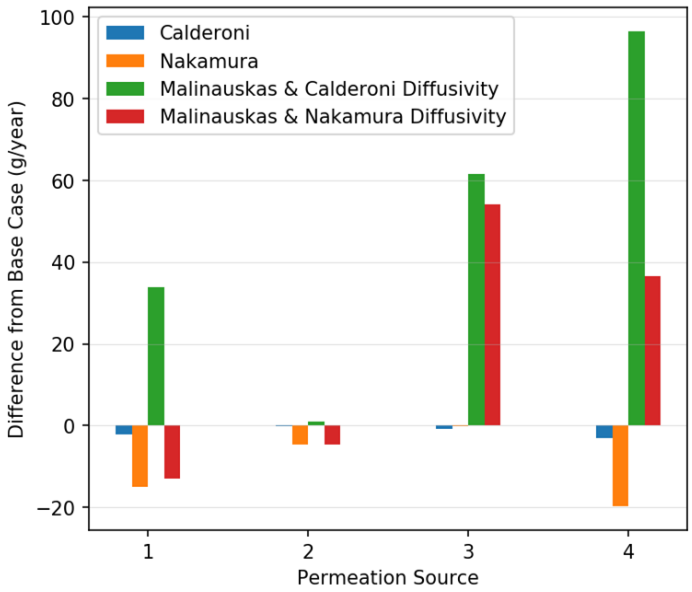

Figure 1.3.10. Differences in tritium permeation rate (grams/year) from base case by varying FLiBe solubility and diffusivity. Permeation rate label descriptions are given in Table 1.3.4.

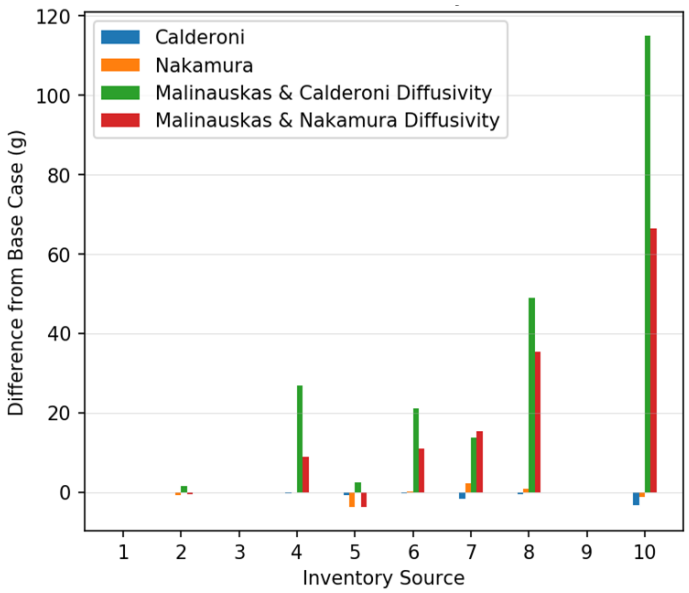

Figure 1.3.11. Differences in tritium inventory (grams) from base case by varying FLiBe solubility and diffusivity. Inventory label descriptions are given in Table 1.3.5.

Figure 1.3.12 and 1.3.13 show the results in change of permeation rates (grams per year) and inventory (grams) of inventory in the simulations due to the change in tritium transport properties of tungsten from those of Frauenfelder [4] to those of Esteban et al. [15]. As tungsten is one of the primary candidates of plasma-facing materials due to its relatively high thermal conductivity and melting point and low sputtering yield [17], the importance of examining the performance of such materials under high tritium flux is paramount to the design and analysis of fusion devices. The purpose of this comparison is to determine the effects of a change in tungsten properties on tritium inventory. A change in these properties is expected to change the mobile and diffusive inventory of tritium at the tungsten FW which may affect the inventory beyond the FW. Examining the change in permeation rates from the base case due to change in tungsten properties, the change in permeation in the outer FLiBe immersion tank wall (permeation location 1), piping systems (permeation location 2) are left relatively unchanged with differences from the base case of only -0.14 grams/year (0.38% of the total base case permeation) and -0.04 grams/year (-0.12% of the total base case permeation), respectively. This can be considered a negligible difference in permeation due to the change in tungsten properties. For the case of the permeation from the HX system, however, is not negligible. Changing the tungsten properties to match those of Esteban et al. (as shown in the “Esteban” data) results in a permeation difference of 141.06 grams/year (382.0% of the total base case permeation). As the tungsten lining in the HX system represents an important tritium barrier at that location, it would be expected that a change in tungsten properties would have a significant effect on permeation. This data indicates that tungsten properties must be carefully measured to determine the effectiveness of this barrier in the HX system.

The change in tritium inventory due to using the differing tungsten properties given in Figure 1.3.13 is now discussed. For all inventory locations (numbers 1-2, 4-8) aside from the FW and inner VV for the upper and lower divertors (inventory location 3) and piping and HX systems (inventory location 9), the individual changes in tritium inventory are less than ± 0.5 grams of tritium. Dividing by the individual base case inventory values for each of these inventory

locations, the individual change in inventory in percent is less than 3.2%. These differences in tritium due to the alternate tungsten properties may be considered negligible. When accounting for the change in inventory at the FW and inner VV for the upper and lower divertors (inventory location 3), however, this represents a change of 74.16 grams of tritium, or a 51.9% increase from the base case value of 142.98 grams. As the tungsten is the plasma-facing material at the FW, it would be expected that changes in tritium transport properties would have a large effect on the inventory of tritium at that location. The HX and piping systems inventory (inventory location 9) had a difference in 16.48 grams of tritium or 8.01% of the base case total inventory. As stated in the discussion on the sensitivity of tungsten permeation due to material properties, this material is a significant tritium barrier in the HX system. A change to its properties would expect to have a significant effect on the inventory in that location which is confirmed by these results, though it is significantly less sensitive than the divertors (inventory location 3). The fact that no other location had a significant change in inventory due to change in tungsten properties is notable; as there is tritium generation in the FLiBe channels behind the FW and inner VV, it appears that the tritium inventory at the Be multiplier and outer VV is more reliant on the tritium generated in the FLiBe channel rather than through the FW and inner VV. This would explain the relatively static tritium inventory despite the tungsten property changes as compared to the large change of inventory in the FW and inner VV.

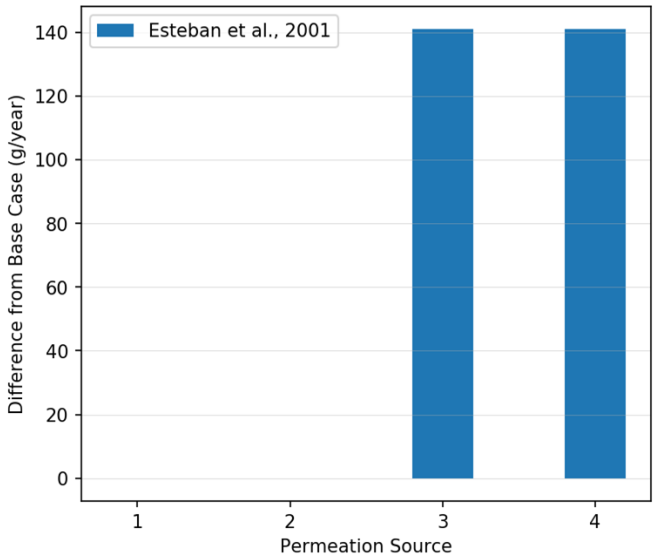

Figure 1.3.12. Differences in tritium permeation rate (grams/year) from base case using tungsten properties from Esteban et al. Permeation rate label descriptions are given in Table 1.3.4.

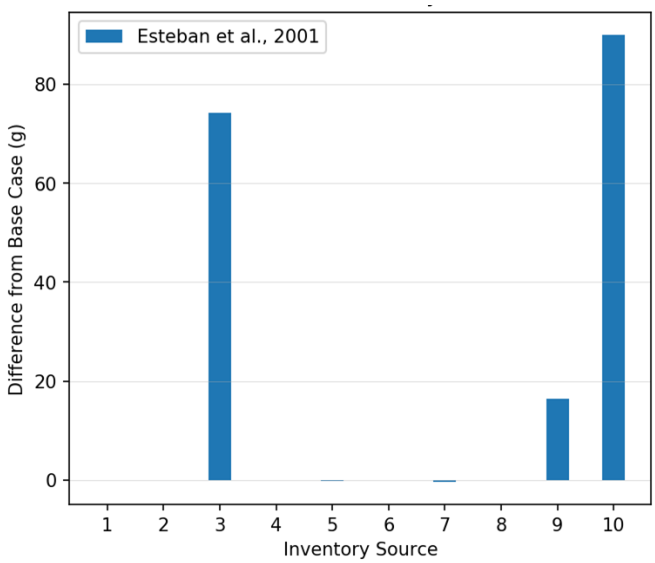

Figure 1.3.13. Differences in tritium inventory (grams) from base case using tungsten properties from Esteban et al. Inventory label descriptions are given in Table 1.3.5.

References:

[1] A. Nakamura, S. Fukada, and R. Nishiumi, "Hydrogen isotopes permeation in a fluoride molten salt for nuclear fusion blanket," *J. Plasma Fusion Res. Series*, vol. 11, no. 25, 2015.

[2] P. Calderoni, P. Sharpe, M. Hara, and Y. Oya, "Measurement of tritium permeation in flibe (2LiF-BeF_2)," *Fusion Eng. Des.*, vol. 83, no. 7-9, pp. 1331-1334, Dec. 2008, doi: 10.1016/j.fusengdes.2008.05.016.

[3] P.W. Humrickhouse and B.J. Merrill, "Revised equation of state for FLiBe in MELCOR," Idaho Nat. Lab., Idaho Falls, ID, USA, Tech. Rep. INL/EXT-17-44148, Dec. 2017.

[4] R. Frauenfelder, "Solution and diffusion of hydrogen in tungsten," *J. Vac. Sci. Technol.*, vol. 6, no. 3, pp. 388-397, May 1969, doi: 10.1116/1.1492699.

[5] R.A. Anderl, D.F. Holland, G.R. Longhurst, R.J. Pawelko, C.L. Trybus, and C.H. Sellers, "Deuterium transport and trapping in polycrystalline tungsten," *Fusion Technol.*, vol. 21, no. 2P2, Mar. 1992, doi: 10.13182/FST92-A29837.

[6] W.M. Robertson, "Hydrogen permeation and diffusion in Inconel 718 and Incoloy 903," *Metall. Trans. A*, vol. 8, pp. 1709-1712, Nov. 1977, doi: 10.1007/BF02646873.

[7] G.A. Esteban, A. Perujo, L.A. Sedano, F. Legarda, B. Mancinelli, and K. Douglas, "Diffusive transport parameters and surface rate constants of deuterium in Incoloy 800," *J. Nucl. Mater.*, vol. 300, no. 1, pp. 1-6, Jan. 2002, doi: 10.1016/S0022-3115(01)00715-2.

[8] A.S. Agazhanov, D.A. Samoshkin, and Y.M. Kozlovskii, "Thermophysical properties of Inconel 718 alloy," *J. Phys.: Conf. Ser.*, vol. 1382, no. 012175, 2019.

[9] V.I. Shapovalov and Y.M. Dukel'skii, "On Be-H phase diagram," (In Russian), *Izvestiya Akademii Nauk SSSR, Metally*, vol. 5, pp. 201-203, 1988.

[10] E. Abramov, M.P. Riehm, D.A. Thompson, and W.W. Smeltzer, "Deuterium permeation and diffusion in high-purity beryllium," *J. Nucl. Mater.*, vol. 175, no. 1-2, pp. 90-95, Dec. 1990, doi: 10.1016/0022-3115(90)90274-Q.
[11] ITER, "Safety analysis data list," G 81 RI 10 03-08-08 W 0.1, Version: 4.0.3 SADL, Sep. 2003.
[12] E.A. Hodille, E. Bernard, S. Markelj, J. Mougenot, C.S. Becquart, R. Bisson, and C. Grisolia, "Estimation of the tritium retention in ITER tungsten divertor target using macroscopic rate equations simulations," *Phys. Scr.*, vol. 2017, Oct. 2017, Art. no. 014033, doi: 10.1088/1402-4896/aa8787.
[13] M.C. Billone, M. Dalle Donne, and R.G. Macaulay-Newcombe, "Status of beryllium development for fusion applications," *Fusion Eng. Des.*, vol. 27, pp. 179-190, Mar. 1995, doi: 10.1016/0920-3796(95)90125-6.
[14] M. Wigram, B. Labombard, M. Umansky, A. Kuang, T. Golfinopolous, J. Terry, D. Brunner, M. Rensink, C. Ridgers, D. Whyte, "Performance assessment of long-legged tightly-baffled diverter geometries in the ARC reactor concept," *Nuclear Fusion* vol. 59, no. 10, 2019. doi: 10.1088/1741-4326/ab394f
[15] G.A. Esteban, A. Perujo, L.A. Sedano, and K. Douglas, "Hydrogen isotope diffusive transport parameters in pure polycrystalline tungsten," *J. Nucl. Mater.*, vol. 295, no. 1, pp. 49-56, May 2001, doi: 10.1016/S0022-3115(01)00486-X.
[16] A.P. Malinauskas, D.M. Richardson, "The solubilities of hydrogen, deuterium, and helium in molten Li2BeF4," *Ind. Eng. Chem. Fundam.*, vol. 13, no. 3, Aug. 1974.
[17] M. Shimada, "Tritium transport in fusion reactor materials," in *Comprehensive Nuclear Materials 2nd Edition*, R.J.M. Konings and R.E. Stoller, Eds., Oxford: Elsevier, 2020.
[18] *Inconel alloy 718*, Special Metals Corporation, Sep. 2007. [Online]. Available: https://www.specialmetals.com/documents/technical-bulletins/inconel/inconel-alloy-718.pdf.
[19] K. Baral, S. San, R. Sakidja, A. Couet, K. Sridharan, and W-Y. Ching, "Temperature-dependent properties of molten Li_2BeF_4 salt using *ab initio* molecular dynamics," *ACS Omega 2021*, vol. 6, no. 30, pp. 19822–19835, Jul. 2021, doi: 10.1021/acsomega.1c02528.
[20] Kuang, A. Q., Cao, N. M., Creely, A. J., Dennett, C. A., Hecla, J., LaBombard, B., Tinguely, R. A., Tolman, E. A., Hoffman, H., Major, M., Ruiz Ruiz, J., Brunner, D., Grover, P., Laughman, C., Sorbom, B. N., & Whyte, D. G. (2018). Conceptual design study for heat exhaust management in the ARC fusion pilot plant. *Fusion Engineering and Design*, *137*, 221–242. https://doi.org/10.1016/j.fusengdes.2018.09.007

2 Impact

2.1 Use of Project Results

Describe how the results obtained contributes to CFS' roadmap. Include a timeline slide pointing out relationships to other DOE programs and SPARC/ARC milestones.

ARC is in the early design stages and one of the major design objectives for the facility is to minimize the required tritium inventory. A major purpose of this study is to conduct preliminary modeling to determine which components and input parameters have the largest impact on required tritium inventory so that further study and development can be focused on those components and input parameters in order to minimize the total tritium inventory.

An initial estimate of tritium inventory in the tokamak and primary heat exchange loop was determined to be 205 g, through preliminary analysis and approximate materials choices, and without design optimization for inventory reduction. This is the first time that an ARC-relevant tritium inventory has been estimated using standard toolsets for torus and salt systems. This preliminary result is consistent with ARC site inventory design targets of hundreds of grams of tritium. The accuracy of this estimate is reduced by uncertainty in the materials and trapping properties of components operating in high neutron fields, including the vacuum vessel and first wall, which dominate stored tritium inventory. Future work should probe the sensitivity of the vacuum vessel wall inventory to uncertainties in trap-site evolution under fusion neutron irradiation specifically, given that the irradiated components comprise such a large fraction of the inventory. Such work could also consider the variation in neutronics-sensitivity of different potential vacuum vessel materials. We also note that these calculations assumed a tungsten first wall and an Inconel vacuum vessel wall. While these materials choices are likely to evolve as ARC continues its design process, we believe that vacuum vessel tritium inventory will be a significant fraction of system tritium inventory even under different material choices. The reason for this is that there is significant plasma-drive flux into the first wall and substrate vacuum vessel behind the first wall.

Another key finding of this study is that tritium permeation rates could be reduced by orders of magnitude using fairly thin tritium permeation barrier coatings, even with imperfect barrier materials like tungsten. This high sensitivity to permeation barrier coatings even at low thickness highlights the importance of barriers in materials choices and component design, particularly the heat exchanger (HX), which is expected to have a high rate of permeation in the absence of any barrier. This analysis investigated the reduction in permeation losses in the HX via permeation barriers, where even thin barriers significantly reduce permeation rates, and shift the dominant permeation location from the HX to other salt-facing components (i.e. the salt-bearing pipes and blanket tank). This analysis suggests that using barriers on these other components could similarly reduce their permeation rates. Other design approaches to reducing permeation rates (such as double walls and secondary containment systems) are also expected to be applicable.

CFS will incorporate these outputs as it continues work to minimize tritium inventory requirements for ARC and understand internal tritium permeation processes. These findings clarify which components contribute most to the tritium inventory and which aspects of the design are the best optimization targets.

2.2 Fusion Energy Impact

Describe how this project will contribute to advancing fusion energy development more generally.

This project has provided an initial estimate of tritium inventories in the tokamak and primary heat exchange loop of an early ARC-like design based on the 2018 published paper by Kuang et al. [1] This estimate supports the possibility of low total site inventories in the compact high-field tokamak fusion approach and identifies the vacuum vessel and first wall as key contributors to tritium inventory. Better understanding tritium inventories and design targets and opportunities supports the fusion industry's design targets as it continues to refine its operational and safety models and engage with regulatory bodies.

These results may also be generally applicable to all fusion concepts which utilize tritium in their fuel cycle.

2.3 Intellectual Property, Publications and Conferences

Identify new IP, publications and conference presentations generated from this project.

There have not been any IP, publications or presentations generated from this project.

References:

[1] Kuang, A. Q., Cao, N. M., Creely, A. J., Dennett, C. A., Hecla, J., LaBombard, B., Tinguely, R. A., Tolman, E. A., Hoffman, H., Major, M., Ruiz Ruiz, J., Brunner, D., Grover, P., Laughman, C., Sorbom, B. N., & Whyte, D. G. (2018). Conceptual design study for heat exhaust management in the ARC fusion pilot plant. *Fusion Engineering and Design*, *137*, 221–242. https://doi.org/10.1016/j.fusengdes.2018.09.007